All-Chalcogenide Ring Fiber Laser

Mohsen Rezaei (mohsen.rezaei@mail.mcgill.ca)
McGill University
Martin Rochette
McGill University

Article

Keywords: all-chalcogenide ring cavity laser, fiber lasers

Posted Date: May 25th, 2021

DOI: https://doi.org/10.21203/rs.3.rs-530080/v1

All-Chalcogenide Ring Fiber Laser

Mohsen Rezaei* **and Martin Rochette**

McGill University, Department of Electrical and Computer Engineering, Montréal, H3A 0E9, Canada
*mohsen.rezaei@mail.mcgill.ca

ABSTRACT

We demonstrate the first all-chalcogenide Brillouin fiber laser as well as the first all-chalcogenide ring cavity laser. The compact device comprises two engineered components: an As_2Se_3 optical fiber coupler combined to an As_2S_3 amplifying fiber. While the coupler simultaneously enables insertion of pump light, extraction of laser light, and the formation of a ring cavity, the amplifying fiber provides nonlinear gain to ensure laser oscillation. Thanks to the strong Brillouin gain of As_2S_3, only $3\ m$ of amplifying fiber is required, thus making a resonant cavity with a free spectral range significantly larger than the Brillouin gain spectrum. The laser therefore naturally enables single longitudinal mode operation without additional filtering device. Acting as a coherence enhancing component, the resulting Brillouin laser benefits of a linewidth reduction factor of 7 with respect to the pump laser. Finally, this laser design is compatible with a broad range of wavelengths that spreads from $1.55\ \mu m$ up to $8\ \mu m$, thanks to its all-chalcogenide structure.

1 Introduction

Coherent laser sources that are characterized by low intensity and frequency noise are of interest in a wide range of applications such as coherent optical communications[1], sensing[2] and microwave photonics[3]. Brillouin fiber lasers (BFLs) are such light sources that are not only coherent but that also act as optical signal processing devices used for coherence enhancement. The spectral linewidth of a BFL generally becomes a narrower version of the laser linewidth used to pump the BFL, thanks to a Brillouin gain spectrum of a few MHz[4,5]. BFLs made of silica require hundreds of meters of cavity length to reach laser threshold, leading to multi-mode operation. Hence, additional filtering is required to enable single-mode operation[6,7]. A simpler version of the silica BFL that naturally leads to single-mode operation, with reduced fiber length and reduced power threshold, can be achieved with the use of a fiber with increased Brillouin gain. Chalcogenide fibers with a large optical nonlinearity of $\sim$3 orders of magnitude beyond silica are interesting candidates to this end[8].

So far, the Brillouin gain of chalcogenide fibers has been studied in a few reports[9–14]. Back in 2005, K. S. Abedin did pioneer work on Brillouin scattering in chalcogenide fibers[9]. He reported stimulated Brillouin scattering in a 5 m long single-mode As_2Se_3 fiber at a wavelength of 1.55 μm, leading to an estimation of the Brillouin gain linewidth of 13.2 MHz and gain coefficient of $6 \times 10^{-9}\ m/W$. In 2006, K. S. Abedin demonstrated stimulated emission from Brillouin amplification in a 2 m long As_2Se_3 fiber[10]. The fiber with polished ends served both as the gain medium and as a Fabry-Perot resonant cavity. A limitation of this demonstration is the lack of an L-I curve to discriminate stimulated emission from laser operation. It is however in 2006 that K. S. Abedin demonstrated the first operational BFL made of chalcogenide fiber. This time, a circular cavity was formed by the combination of an As_2Se_3 gain fiber, a silica optical fiber coupler (OFC), and two optical circulators[11]. The multimode laser had a threshold pump power of 35 mW. In 2012, K. Tow et al. employed a 3 m long suspended-core As_2Se_3 fiber to form the first single-mode ring cavity BFL[12]. Lasing was observed for a pump power of 22 mW at a wavelength of 1.55 μm. In the same year, K. Tow et al. demonstrated a second BFL with a similar ring cavity configuration but replacing the gain medium by a 3 m long microstructured $Ga_{10}As_{22}Se_{68}$ fiber, leading to a laser power threshold of 6 mW[13]. In contrast with every previous demonstrations at a wavelength of 1.55 μm, K. Hu et al. presented in 2014 the first chalcogenide-based BFL at an operating wavelength of 1.95 μm[14]. The laser was made of a 1.5 m long As_2Se_3 suspended-core fiber and operated at a power threshold of 52 mW. A common trait of every chalcogenide BFL reported thus far is the ring cavity made of a hybrid combination of silica-based components such as OFCs and optical circulators coupled to a chalcogenide gain fiber. The operating wavelength range of those BFLs is thus limited to the common transparency window of silica and chalcogenide glass, that is at most $\sim$2 μm in the long wavelength side.

Recently, the first single-mode OFCs made of chalcogenide fibers have been demonstrated, providing a possibility to build all-chalcogenide fiber cavities[15,16]. In this article, we propose the first all-chalcogenide BFL, as well as the first all-chalcogenide ring cavity. The BFL includes an As_2Se_3 OFC to form a resonant ring cavity, in addition to an As_2S_3 optical fiber to provide Brillouin amplification. The BFL is single-mode owing to its short cavity length and spectrally narrow Brillouin gain. While the laser used to pump this BFL has a linewidth of 14.4 MHz, the narrow Brillouin gain provided by the BFL enables a 7-fold coherence enhancement, leading to a BFL linewidth of 1.9 MHz. This fiber laser is expected to be compatible over a broad

range of wavelengths that spreads from 1.5 μm up to 8 μm, thanks to the all-chalcogenide structure of the resonant cavity.

2 Experiment and Results

The amplifying fiber used in this experiment is an As_2S_3 fiber with core/cladding diameter of 8.5 μm/170 μm and a numerical aperture of 0.24. The fiber is 3 m long with a transmission loss of 0.7 dB/m. A first experiment is set to measure the Brillouin gain coefficient (g_B) of this fiber. Figure 1 shows a schematic of the setup. Continuous wave light from an external cavity laser at a wavelength of 1550 nm is launched into the As_2S_3 fiber via a polarization controller and an optical circulator. The polarization controller is used to maximize Brillouin emission via linearly polarized pump light whereas the circulator enables to simultaneously inject and collect light to/from the As_2S_3 fiber. The As_2S_3 fiber is coupled to the circulator via an SMF-28 pigtail and UV-cured epoxy, leading to a coupling loss of 1 dB. The far-end of the As_2S_3 fiber is angle-polished to prevent Fresnel back reflection. An optical spectrum analyzer (OSA) is used for light analysis purposes. Figure 2a shows the optical spectrum of the backscattered Brillouin amplified spontaneous emission at an injected pump power of of 250 mW. The Brillouin spectrum is also accompanied with pump signal reflected from the silica-As_2S_3 interface with a reflection coefficient of 5%. Figure 2b shows the power of back-propagating Brillouin light as a function of pump power launched into the As_2S_3 fiber. Brillouin light is measured specifically at the Brillouin wavelength with the use of the OSA to ensure a good isolation from back-reflected pump light. This Brillouin profile decomposes in to two regimes: spontaneous emission of Brillouin light at low pump power up to $\sim$200 mW and amplified spontaneous emission of Brillouin light at pump power of $\sim$200 mW and up. Using $P_0 \approx 200$ mW and small-signal steady-state theory of stimulated Brillouin scattering[17], the Brillouin gain coefficient of the As_2S_3 fiber is evaluated with

$$g_B \cong \frac{21A_{eff}}{KL_{eff}P_0}, \tag{1}$$

where $A_{eff} = 40.2\ \mu m^2$ is the effective mode area, and $L_{eff} = (1-e^{-\alpha L})/\alpha = 2.3\ m$ is the effective interaction length. The constant K is equal to 1 if the fiber is polarization-maintaining and 0.5 if not, which is the case here. With the values given above, the Brillouin gain coefficient is $g_B \approx 3.7 \times 10^{-9}\ m/W$, in accordance with previous report[5].

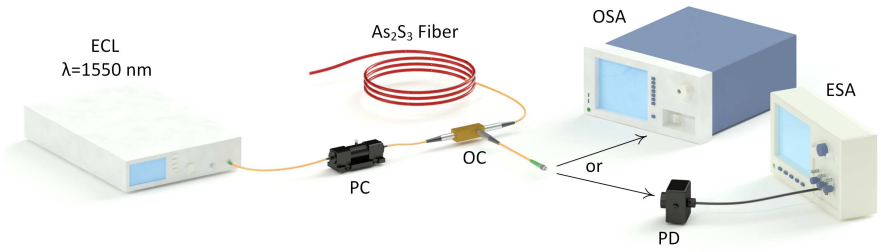

Figure 1. Schematic of the setup used for measuring Brillouin gain coefficient and Brillouin gain spectrum. ECL: external cavity laser; PC: polarization controller; OC: optical circulator; OSA: optical spectrum analyzer; PD: photodetector; ESA: electrical spectrum analyzer.

Brillouin frequency shift and Brillouin gain bandwidth are also measured from an heterodyne technique. This time, the setup of Fig. 1 is used along with a photodiode (PD) and electrical spectrum analyzer (ESA) on the detection end. Brillouin signal from the As_2S_3 fiber along with residual pump signal reflected from the silica-As_2S_3 interface are collected by the PD-ESA pair. The pump signal has a full width at half maximum (FWHM) bandwidth of 24 KHz, considerably smaller than the expected Brillouin gain spectrum. Figure 3 shows the RF spectrum of the beating between the pump and Brillouin signals. The Brillouin gain spectrum shows a FWHM Brillouin gain bandwidth of $\Delta\nu_B = 14.9\ MHz$ with a frequency offset with respect to pump of 7.93 GHz, as expected from previous measurement[5]. To compare with this experimental result, the Brillouin gain spectrum is considered to have a Lorentzian profile with a bandwidth given by[18]:

$$\Delta\nu_B = \frac{2\pi M_1}{c\lambda_p^2 g_B}, \tag{2}$$

where $M_1 = 619 \times 10^{-8}\ m^2s/kg$[19] is the As_2S_3 figure of merit related to the acousto-optic diffraction efficiency, $c = 3 \times 10^8\ m/s$ is the speed of light and $\lambda_p = 1550\ nm$ is the pump wavelength. From the measured value of $g_B = 3.7 \times 10^{-9}\ m/W$, the theoretical Brillouin gain bandwidth is estimated at $\Delta\nu_B = 14.6\ MHz$, in good agreement with the measurement.

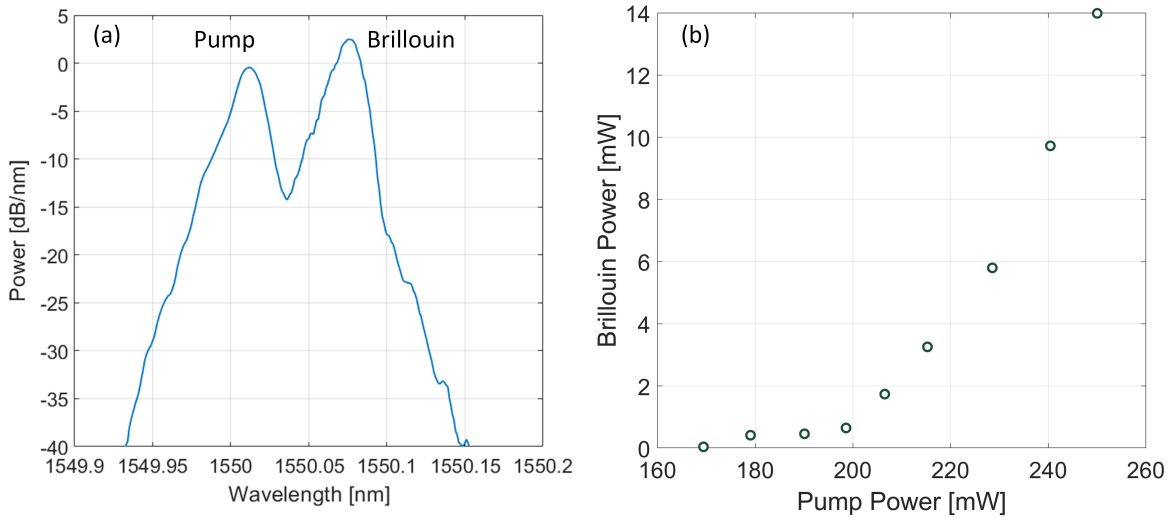

Figure 2. (a) Optical spectrum of the pump signal and Amplified Spontaneous emission at the Brillouin wavelength. (b) Brillouin power as a function of injected pump power.

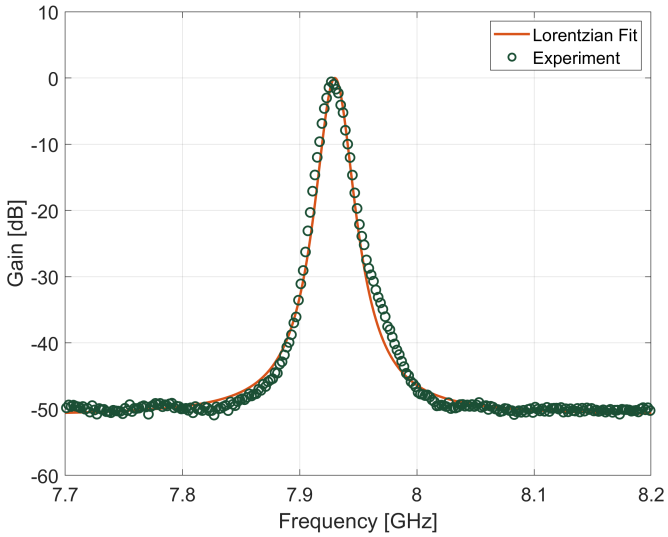

Figure 3. Brillouin gain spectrum.

Now that the gain fiber has been characterized, the BFL is to be built. After the Brillouin gain fiber, the second component of the ring cavity is an As_2Se_3 OFC. To make the OFC, two identical pieces of As_2Se_3 fiber with a numerical aperture of 0.12 and core/cladding diameters of 6 μm/170 μm are pretapered, cleaved, polished and coupled to SMF-28 with UV-cured epoxy. Both As_2Se_3 fibers are then placed side by side on a tapering setup, heated and adiabatically stretched to form a single-mode OFC. Figure 4 shows a schematic of the tapering setup. A computer precisely controls the pulling stages that stretch both fibers, the translation stage of the heating element that maintains a hot-zone of variable length, as well as the temperature of the heating element. While tapering, continuous wave laser light at a wavelength of 1550 *nm* is launched into one of the As_2Se_3 fibers and both outputs are monitored using two power meters. Figure 5 shows the coupling ratio of an As_2Se_3 OFC as a function of extension. The extension is the distance that PS1 and PS2 have moved away from each other in the tapering process. This typical profile of coupling ratio versus extension will be useful in the next steps to come because the coupler will be fabricated *in situ* to form a ring resonant cavity.

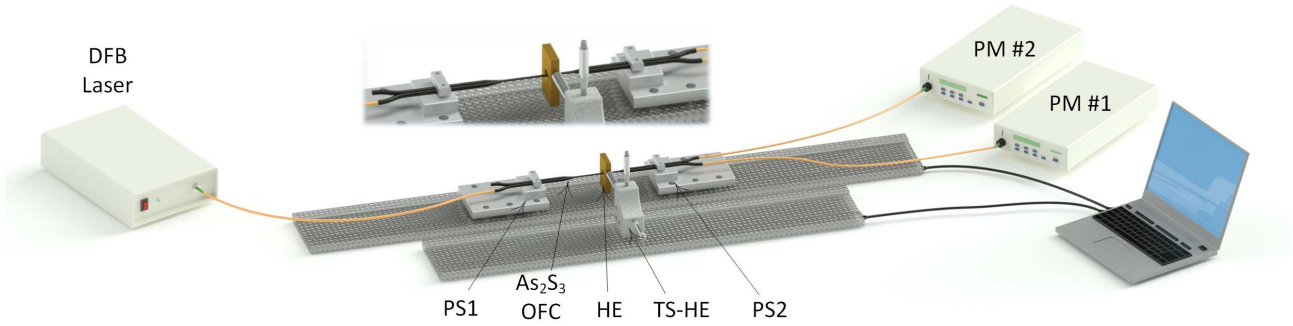

Figure 4. Schematic of the tapering setup. PS: pulling stage; OFC: optical fiber coupler; HE: heating element; TS-HE: translation stage of heating element; PM: power meter.

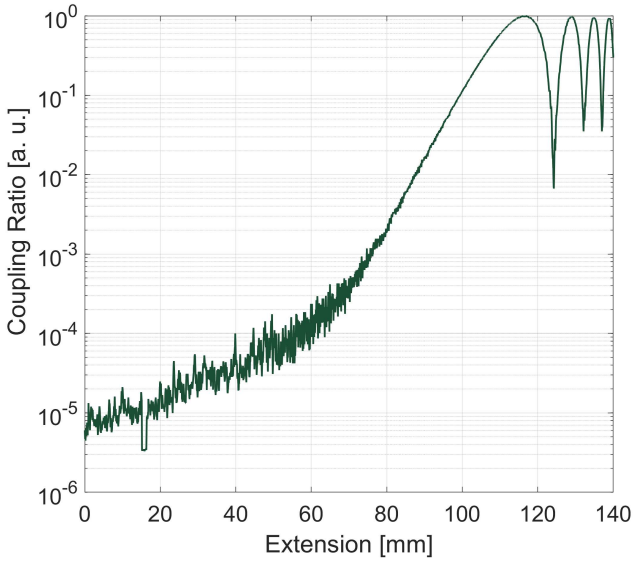

Figure 5. Coupling ratio of an As_2Se_3 OFC as a function of extension in the tapering setup of fig. 4.

The BFL is now ready to be assembled from the combination of the As_2S_3 fiber as the gain medium, and an As_2Se_3 OFC that will close the ring cavity. For this purpose, a train of 5 fibers in series is assembled. Two identical pieces of 10 *cm* long As_2Se_3 fiber are coupled to both ends of the 3.0 *m* long As_2S_3 fiber. Then, the free-end of each As_2Se_3 fiber is also coupled to SMF-28 pigtails. Optical joints in between each pairs of fibers is performed by polishing and UV-cured epoxy application. Insertion loss of silica-As_2Se_3 and As_2S_3-As_2Se_3 joints are $\sim$1 *dB* and $\sim$1.3 *dB*, respectively. Figure 6a shows the train of fibers prior to tapering, which consists of the ordered sequence of an SMF-28 pigtail, a section of As_2Se_3 fiber, a section of As_2S_3 fiber, a section of As_2Se_3 fiber, and an SMF-28 pigtail. To fabricate the ring cavity, both As_2Se_3 fibers of the train are placed side by side on the tapering setup by looping the train of fibers on itself once, and transformed into an OFC following the approach presented above. Figure 6b shows the train of fibers on the tapering setup.

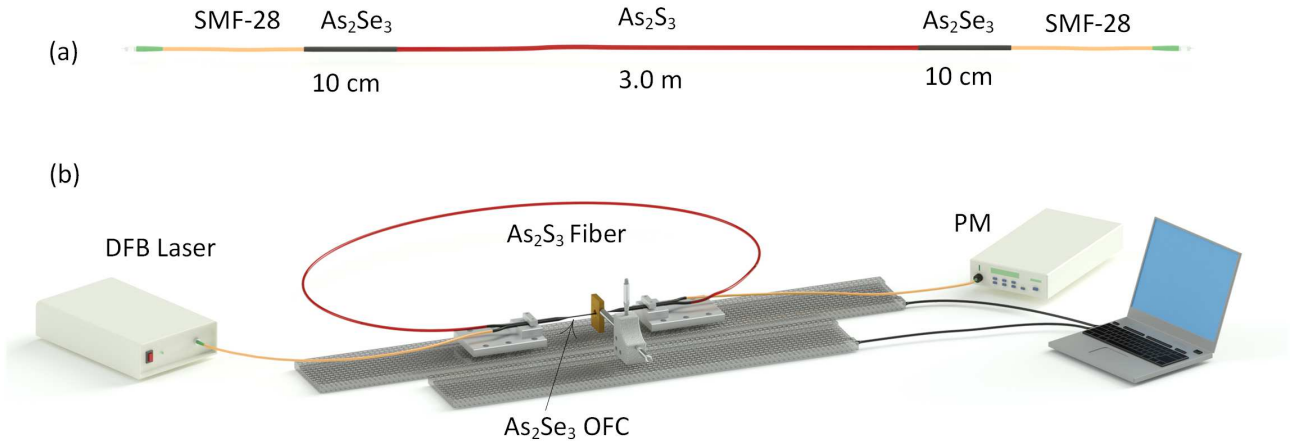

Figure 6. (a) Train of fibers prior to OFC fabrication. (b) Train of fibers rolled in a loop on the tapering setup. OFC: optical fiber coupler; PM: power meter.

During tapering, continuous wave laser light at a wavelength of 1550 *nm* is launched into the cavity and monitored at the cross port of the OFC using a power meter. The monitored power is the response of the resonant cavity as a function of the coupling coefficient of the OFC. Figure 7 shows the transmitted power through the cavity as a function of extension alongside the analytical simulation with a good accordance. At initial stages of tapering there is no coupling in between ports of the OFC. Therefore, the input light passes through both As_2Se_3 fibers and the As_2S_3 fiber in between them, facing an insertion loss of $\sim$5 dB. As tapering proceeds, the distance between the core of both As_2Se_3 fibers reduces, leading to a gradual overlap in between the modes of both fiber cores, and thus inducing cross-coupling. The coupling becomes noticeable at an extension of $\sim$90mm, where some of the input light directly couple to the resonator output without passing through the As_2S_3 fiber. Therefore, the coupled light faces smaller insertion loss and the output power increases. The tapering process is stopped at an extension of 110 *mm* which results in a 70:30 OFC, with 70% of the input power going through the cavity. The transmission of the cavity as a function of extension is retrieved from the theoretical transmission function[20,21]:

$$T = \left|\frac{e^{-j\beta L-\alpha L}(cos(K_eZ)+j(\delta_a/K_e)sin(K_eZ))}{1-e^{-j\beta L-\alpha L}(jk/K_e)sin(K_eZ)}\right|^2, \tag{3}$$

where $\beta = 9.73\times10^6\ rad/m$ is propagation constant, $\alpha = 0.15\ Np/m$ is attenuation coefficient, $L = 3\ m$ is the As_2S_3 fiber length, K_e is effective coupling coefficient, Z is the coupler length, $\delta_a = 0.4$ is asymmetry between the two cores of the OFC. K_e and Z are functions of extension and $C = sin(K_eZ)$ where C is the coupling ratio. The coupling ratio is obtained from Fig. 5.

Figure 8 shows a schematic of the fabricated BFL. The cavity has a length of 3.2 *m*, including 3.0 *m* of As_2S_3 fiber and 0.2 *m* of As_2Se_3 fiber which has expanded from tapering, leading to a ring cavity with a free spectral range of 39 MHz. With the Brillouin gain bandwidth of 14.9 MHz, this free spectral range guarantees the single-mode operation of the BFL. In order to determine the BFL threshold power, continuous wave light from a distributed feedback laser at a wavelength of 1550.45 *nm* is launched into the resonant cavity and the Brillouin signal is monitored using an OSA. Brillouin light is measured specifically at the Brillouin wavelength with the use of the OSA to ensure a good isolation from back-reflected pump light. Figure 9a shows the Brillouin power as a function of pump power. The BFL displays a threshold power of $P_{th} = 62\ mW$ for the pump power delivered to the OFC input. Figure 9b shows optical spectra of the BFL output for pump powers of 60 mW and 73 mW. The signal at the wavelength of $\sim$1550.46 *nm* is the pump after Fresnel reflection from the silica-As_2Se_3 interface. This reflection could be suppressed using antireflection coatings or using angled-polished fibers before splicing. The Brillouin signal is observed at a wavelength of 1550.52 *nm*. The 0.06 *nm* spectral offset between the pump and Brillouin signals corresponds to the Brillouin offset 7.9 GHz, as observed in the measurement above.

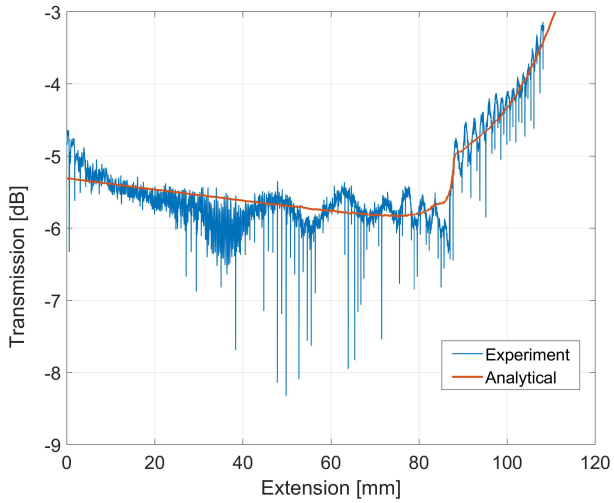

Figure 7. Cavity transmission as a function of extension.

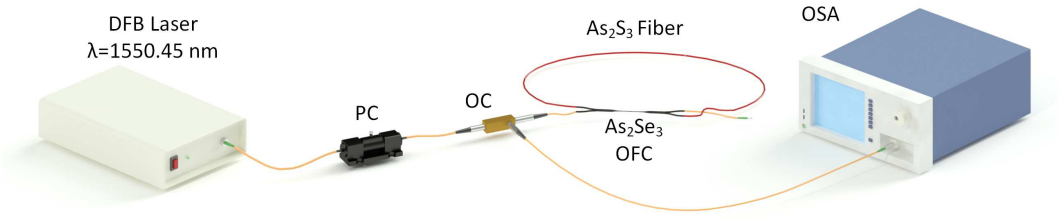

Figure 8. Schematic of the single-frequency Brillouin lasing using chalcogenide ring cavity. PC: polarization controller; OC: optical circulator; OSA: optical spectrum analyzer; OFC: optical fiber coupler.

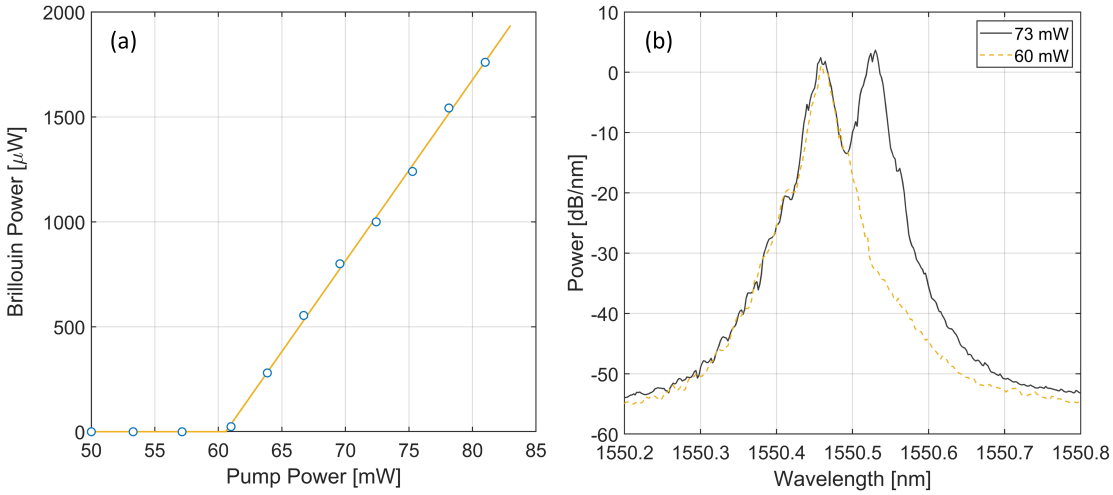

Figure 9. (a) BFL power as a function of pump power launched into the ring cavity. (b) Optical spectra of the BFL for a pump power of $60\,mW$ and $73\,mW$.

Coherence enhancing of the BFL is investigated by optical heterodyne to reveal the linewidth of both pump and Brillouin signals. Figure 10 shows a schematic of the characterization setup. An external cavity laser at a wavelength of 1550.49 *nm* with a narrow linewidth (24 KHz) with respect to the pump and Brillouin signals is used as a local oscillator (LO). The LO,

Brillouin signal from the resonant cavity and pump signal reflected from the interface of silica-As_2Se_3, are combined via a 3 dB coupler, sent into a PD and monitored using an ESA.

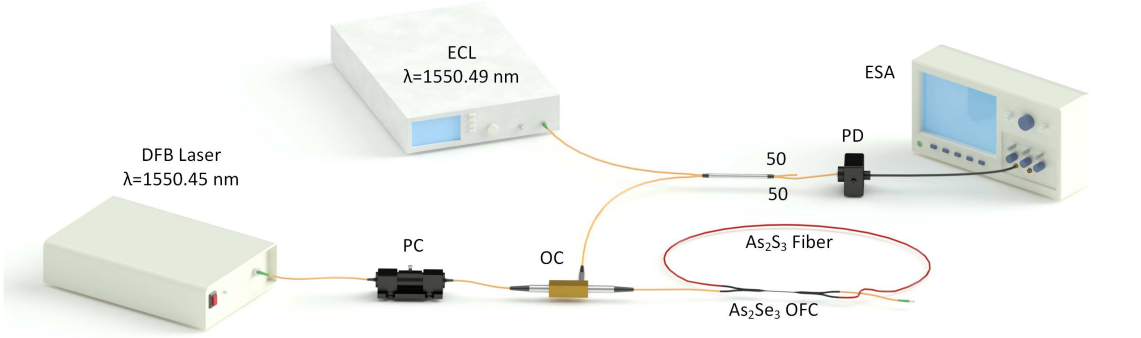

Figure 10. Schematic of the optical heterodyne setup. PC: polarization controller; OC: optical circulator; OFC: optical fiber coupler; PD: photodetector; ESA: electrical spectrum analyzer.

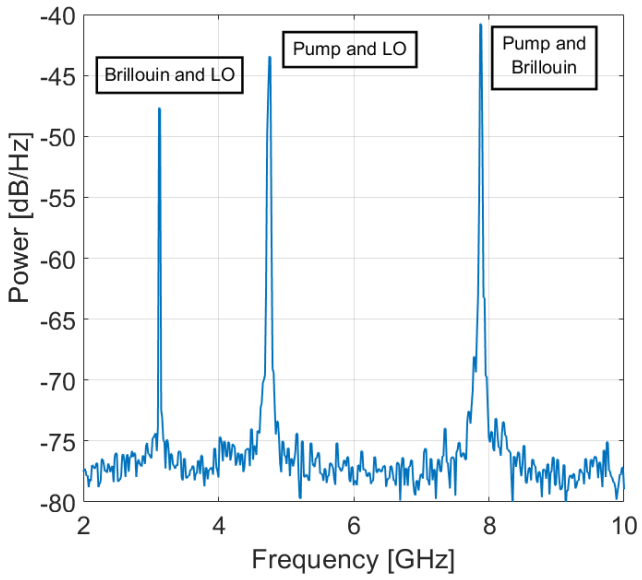

Figure 11. RF spectrum of the beating between local oscillator (LO), pump and Brillouin signals.

Figure 11 shows the RF beating in between the BFL, pump laser, and LO. The signal at $\sim$3.1 GHz represents the beating in between LO and Brillouin signal, the peak at $\sim$4.8 GHz represents the beating in between LO and pump, and the third signal at $\sim$7.9 GHz represents the beating in between pump and Brillouin signals.

Figure 12a and 12b show the RF spectrum of the pump and Brillouin signals, respectively. The FWHM bandwidth of pump signal is 14.4 MHz, whereas for the Brillouin signal it reduces to 1.9 MHz. The BFL therefore has narrowed the pump laser signal by a factor of $>$7. Moreover, the single-peaked Brillouin spectrum in figure 12b demonstrates that the BFL is single-mode.

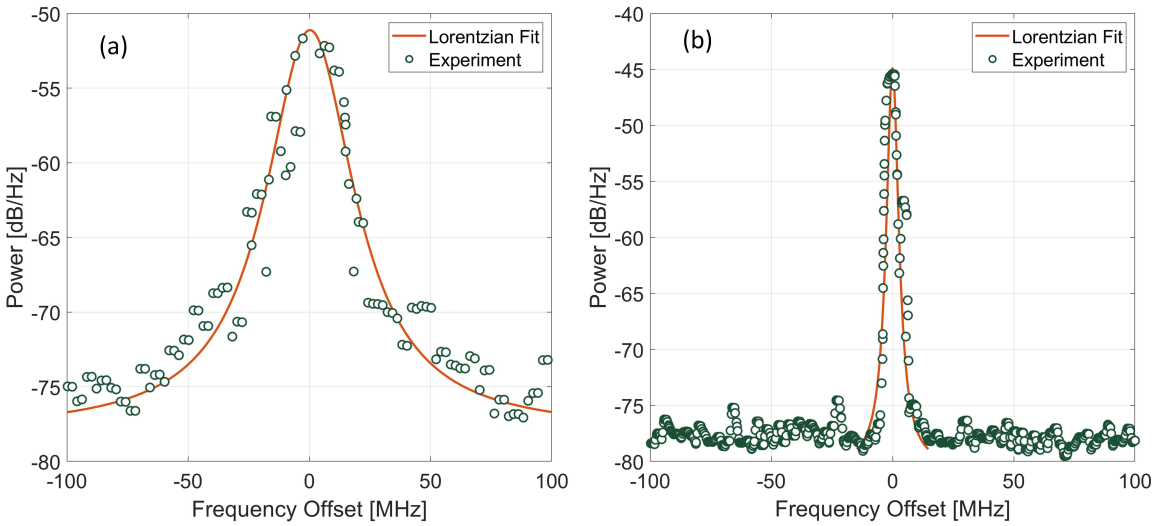

Figure 12. RF spectrum of the (a) pump and (b) Brillouin signals.

The beating frequency ν_B in between the pump and Brillouin signals was also measured for different pump wavelengths varying from 1540 nm to 1570 nm. Figure 13 shows ν_B as a function of pump wavelength. The beat frequency is theoretically calculated from[18]:

$$\nu_B = 2n_p\nu_A/\lambda_p, \tag{4}$$

where n_p is the effective mode index at the pump wavelength λ_p, and ν_A is the acoustic velocity. Using the slope of the ν_B vs λ_p curve and $n_p = 2.4$, the acoustic velocity in As_2S_3 fiber is calculated $\nu_A = 2561\ m/s$, in good agreement with ref.[19].

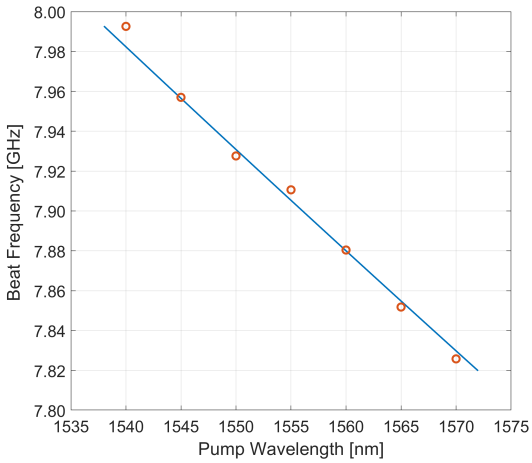

Figure 13. Beat frequency as a function of pump wavelength.

3 Conclusion

In conclusion, we demonstrated the first all-chalcogenide BFL as well as the first all-chalcogenide ring cavity laser. The BFL operates in single longitudinal mode. It includes an As_2S_3 optical fiber serving as a gain medium and an As_2Se_3 OFC in order to form the resonant cavity. The BFL has a threshold power of $P_{th} = 62\ mW$ for the pump power delivered to the input of the ring cavity. The BFL narrows down the linewidth of the pump signal by a factor of >7. We also characterized the Brillouin gain of As_2S_3 fiber showing a $g_B \approx 3.7 \times 10^{-9}\ m/W$ and Brillouin gain bandwidth of $\Delta\nu_B = 14.9\ MHz$.

References

1. Kikuchi, K. Fundamentals of coherent optical fiber communications. *Journal of Lightwave Technology* **34**, 157–179 (2015).
2. Banakh, V. & Smalikho, I. *Coherent Doppler wind lidars in a turbulent atmosphere* (Artech House, 2013).
3. Fortier, T. M., Kirchner, M. S., Quinlan, F., Taylor, J., Bergquist, J., Rosenband, T., Lemke, N., Ludlow, A., Jiang, Y., Oates, C. *et al.* Generation of ultrastable microwaves via optical frequency division. *Nature Photonics* **5**, 425–429 (2011).
4. Nikles, M., Thevenaz, L. & Robert, P. A. Brillouin gain spectrum characterization in single-mode optical fibers. *Journal of Lightwave Technology* **15**, 1842–1851 (1997).
5. Sanghera, J. S., Shaw, L. B., Pureza, P., Nguyen, V. Q., Gibson, D., Busse, L., Aggarwal, I. D., Florea, C. M. & Kung, F. H. Nonlinear properties of chalcogenide glass fibers. *International Journal of Applied Glass Science* **1**, 296–308 (2010).
6. Zhao, J., Zhang, C., Ji, Z., Miao, C., Gu, H., Tong, Z., Sun, X. & Bai, J. Widely tunable ultra-narrow linewidth single-longitudinal-mode brillouin fiber laser with low threshold. *Laser Physics* **24**, 105102 (2014).
7. Kayes, M. I. & Rochette, M. Optical frequency comb generation with ultra-narrow spectral lines. *Optics letters* **42**, 2718–2721 (2017).
8. Beugnot, J. C., Ahmad, R., Rochette, M., Laude, V., Maillotte, H. & Sylvestre, T. Reduction and control of stimulated brillouin scattering in polymer-coated chalcogenide optical microwires. *Optics letters* **39**, 482–485 (2014).
9. Abedin, K. S. Observation of strong stimulated brillouin scattering in single-mode as 2 se 3 chalcogenide fiber. *Optics Express* **13**, 10266–10271 (2005).
10. Abedin, K. S. Single-frequency brillouin lasing using single-mode as2se3 chalcogenide fiber. *Optics express* **14**, 4037–4042 (2006).
11. Abedin, K. S. Brillouin amplification and lasing in a single-mode as2se3 chalcogenide fiber. *Optics letters* **31**, 1615–1617 (2006).
12. Tow, K. H., Léguillon, Y., Besnard, P., Brilland, L., Troles, J., Toupin, P., Méchin, D., Trégoat, D. & Molin, S. Relative intensity noise and frequency noise of a compact brillouin laser made of as38se62 suspended-core chalcogenide fiber. *Optics Letters* **37**, 1157–1159 (2012).
13. Tow, K. H., Léguillon, Y., Fresnel, S., Besnard, P., Brilland, L., Méchin, D., Trégoat, D., Troles, J. & Toupin, P. Linewidth-narrowing and intensity noise reduction of the 2nd order stokes component of a low threshold brillouin laser made of ge 10 as 22 se 68 chalcogenide fiber. *Optics express* **20**, B104–B109 (2012).
14. Hu, K., Kabakova, I. V., Büttner, T. F., Lefrancois, S., Hudson, D. D., He, S. & Eggleton, B. J. Low-threshold brillouin laser at 2 μm based on suspended-core chalcogenide fiber. *Optics letters* **39**, 4651–4654 (2014).
15. Tavakoli, F., Rekik, A. & Rochette, M. Broadband and wavelength-dependent chalcogenide optical fiber couplers. *IEEE Photonics Technology Letters* **29**, 735–738 (2016).
16. Rezaei, M. & Rochette, M. All-chalcogenide single-mode optical fiber couplers. *Optics letters* **44**, 5266–5269 (2019).
17. Smith, R. G. Optical power handling capacity of low loss optical fibers as determined by stimulated raman and brillouin scattering. *Applied optics* **11**, 2489–2494 (1972).
18. Agrawal, G. P. *Nonlinear Fiber Optics, 6th ed.* (Elsevier, 2019).
19. Dixon, R. Photoelastic properties of selected materials and their relevance for applications to acoustic light modulators and scanners. *Journal of Applied Physics* **38**, 5149–5153 (1967).
20. Agrawal, G. P. *Applications of nonlinear fiber optics, 3rd ed.* (Academic press, 2020).
21. Stokes, L. F., Chodorow, M. & Shaw, H. J. All-single-mode fiber resonator. *Optics Letters* **7**, 288–290 (1982).

4 Funding

Collaborative Research and Development Grants Program of the Natural Sciences and Engineering Research Council of Canada (NSERC).

5 Acknowledgments

The authors are thankful to CorActive for the As_2S_3 and As_2Se_3 fibers utilized in this work.

Author contributions statement

Must include all authors, identified by initials, for example: A.A. conceived the experiment(s), A.A. and B.A. conducted the experiment(s), C.A. and D.A. analysed the results. All authors reviewed the manuscript.

Additional information

To include, in this order: **Accession codes** (where applicable); **Competing interests** (mandatory statement).

The corresponding author is responsible for submitting a competing interests statement on behalf of all authors of the paper. This statement must be included in the submitted article file.

Supplementary Files

This is a list of supplementary files associated with this preprint. Click to download.

- nrlasingreporting1.pdf